Proceedings of the ASME 2017 36th International Conference on Ocean, Offshore and Arctic Engineering
OMAE2017
June 25-30, 2017, Trondheim, Norway

OMAE2017-62507

TRANSVERSE DEFORMATION OF PRESSURISED PIPES WITH DIFFERENT AXIAL LOADS

Martin Kristoffersen*
Tore Børvik
Magnus Langseth
Structural Impact Laboratory (SIMLab)
Centre for Advanced Structural Analysis (CASA)
Norwegian University of Science and Technology
Rich. Birkelands vei 1, NO-7491 Trondheim, Norway
E-mail: martin.kristoffersen@ntnu.no

Håvar Ilstad
Erik Levold
Statoil ASA
Research Centre Trondheim
Marine Facilities and Pipeline Technology
Pb. 2470, NO-7053 Ranheim, Norway
E-mail: hil@statoil.com

ABSTRACT

Pipelines residing on the seabed are exposed to various hazards, one of them being denting, hooking and release of the pipeline by e.g. anchors or trawl gear. As a pipeline is displaced transversely in a hooking event, an axial tensile load resisting the displacement builds up in the pipeline. This study examines the effect of applying three different axial loads (zero, constant, and linearly increasing) to a pipe while simultaneously deforming it transversely. A fairly sharp indenter conforming to the prevailing design codes was used to deform the pipes. These three tests were repeated with an internal pressure of about 100 bar for comparison. Adding an axial load appeared to increase the pipe's stiffness in terms of the force-displacement curve arising from deforming the pipe transversely. The internal pressure also increased the stiffness, and produced a more local dent in the pipe compared with the unpressurised pipes. All tests were recreated numerically in finite element simulations. Generally, the results of the simulations were in good agreement with the experiments.

INTRODUCTION

Pipelines are an integral part of the offshore industry and will continue to be so for the foreseeable future. Multiple hazards are present in the waters [1], and close to the coast pipelines may suffer impact and hooking by e.g. anchors or trawl gear [2]. An initial impact typically causes a dent in the pipe, and if the impacting object hooks the pipeline it may displace it significantly, during which membrane forces arise in the pipeline. When the pipeline is released, it recoils back towards its initial position, thereby creating a complex load history.

The open literature provides studies on impact against tubular structures of various character, ranging from rectangular cross-sections [3] to the more complicated T-joints [4]. Circular cross-sections are the most common, and are studied experimentally [5], theoretically [6] and numerically [7]. Inclusion of pressure in pipes during impact has also been investigated [8, 9]. Manes et al. [10] attempted to recreate the loading sequence of impact, hooking and subsequent release of an X65 pipline by subjecting strips taken from an actual offshore pipeline to quasi-static three point bending tests. The strips were then pulled straight and checked for fracture, which was present only as minor surface cracks without exerting any influence on the force-displacement curves. Later, simply supported X65 steel pipes were subjected to a dynamic impact before being pulled straight in quasi-static tension to emulate the release after hooking [11]. Here, fracture was a dominant part of the problem. When investigating fracture, dynamic effects from springback can be important [8, 12].

During an impact and hooking event the pipeline will deform locally and a dent will form under the impactor, and large

*Corresponding author

displacements may be attained during hooking [13]. With increasing displacements, the axial membrane forces resisting the displacement will naturally increase. Through displacement controlled quasi-static experiments, this study investigates the effect of axial tension loading and internal pressure on transverse deformation represented by force-displacement curves. Six seamless pipes made from an X65 offshore steel were deformed by a three-point bending procedure while simultaneously applying one of three different axial load curves – these being no axial load, a constant axial load, and an axial load increasing linearly in proportion with the transverse deformation. The main result from this test series was that adding an axial load increased the pipe's resistance to transverse bending. Three additional pipes subjected to the same loading sequences were tested with an internal pressure of 100 bar, resulting in an increased force level during transverse deformation and a reduction of the cross-sectional deformation, confirming the results by Jones and Birch [1].

Finally, these experiments have been recreated numerically using the finite element software ABAQUS [14]. Results in terms of global force-displacement curves are generally in good agreement with the experimental data, as are the final deformations of the pipe. Both the effects of the axial load and the internal pressure was captured in the simulations.

MATERIAL CHARACTERISATION

Description

The material in the pipes used in this study is an X65 grade steel, a material widely used in pipelines conveying oil and/or gas [15]. According to the material inspection certificate, the yield strength is 450 MPa and the ultimate tensile strength is 535 MPa. Young's modulus is 208 000 MPa. The pipes used are made seamless by utilising the Mannesmann effect [16], and are supplied by Tenaris, Argentina.

Tension tests

Quasi-static material tests investigating the homogeneity and anisotropy of this material have been carried out [11], and are succinctly summarised here. Axisymmetric specimens of geometry as shown in Fig. 1 were loaded to failure in tension at quasi-static strain rate and at room temperature. By using a laser-based measuring device [17], the minimum diameter of the material test specimens was recorded continuously during testing. This enables calculation of the true stress and true strain beyond necking, and a representative curve is shown as a solid line in Fig. 2.

For engineering and design purposes, the material appears both homogeneous and isotropic. Based on values from 12 tests, the material yields at 478 ± 15 MPa and has an ultimate tensile strength of 572 ± 14 MPa. It strain hardens to a true peak stress of $1\,314 \pm 12$ MPa and fails at a true strain of 1.61 ± 0.03 by

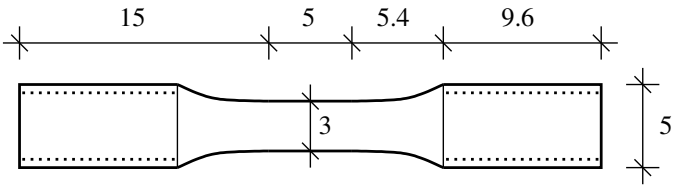

FIGURE 1. TENSION TEST SPECIMEN GEOMETRY [mm].

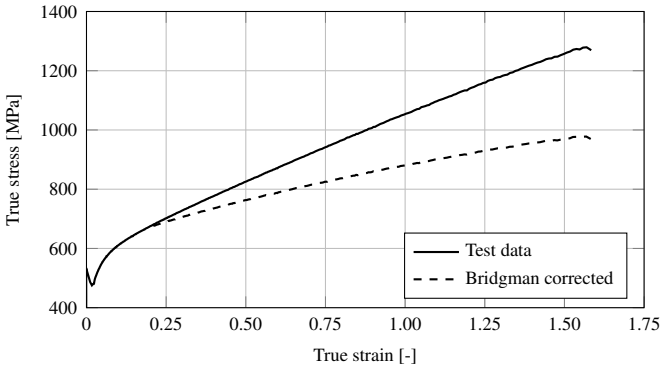

FIGURE 2. A REPRESENTATIVE TRUE STRESS-TRUE STRAIN CURVE (SOLID) FROM THE TENSION TESTS, ALONG WITH CORRESPONDING BRIDGMAN CORRECTED DATA (DASHED).

a ductile cup-and-cone fracture. Microscope images revealed a dimpled fracture surface arising from void coalescence [11].

Constitutive relation

To model the X65 material for use in finite elements simulations, J2 flow theory is used with isotropic power-law hardening. Kinematic hardening is not included as the global response differs only marginally in similar cases [18]. The von Mises equivalent stress σ_{eq} is given as a function of the deviatoric part $\boldsymbol{\sigma}^{\text{dev}}$ of the Cauchy stress tensor $\boldsymbol{\sigma}$,

$$\sigma_{\text{eq}}(\boldsymbol{\sigma}) = \sqrt{\frac{3}{2}\boldsymbol{\sigma}^{\text{dev}} : \boldsymbol{\sigma}^{\text{dev}}} \tag{1}$$

The flow stress σ_{flow} is expressed as

$$\sigma_{\text{flow}}\left(\varepsilon_{\text{eq}}\right) = A + B\varepsilon_{\text{eq}}^{n} \tag{2}$$

where ε_{eq} is the equivalent plastic strain, and A, B and n are material constants. While strain rate effects have been shown to be important to include in impact simulations [4], no strain rate effects are accounted for herein as the tests conducted are carried

out at quasi-static strain rates (less than 10^{-3} s^{-1}). Also, isothermal conditions are assumed. Then, from Eq. (1) and Eq. (2), the yield function f becomes

$$f\left(\boldsymbol{\sigma}, \varepsilon_{\text{eq}}\right) = \sigma_{\text{eq}}\left(\boldsymbol{\sigma}\right) - \sigma_{\text{flow}}\left(\varepsilon_{\text{eq}}\right) \leq 0 \tag{3}$$

The initial size of the yield surface, i.e. when the equivalent plastic strain is zero, is given by the constant A. B and n are related to the strain hardening.

Identification of material constants

To determine the equivalent stress σ_{eq} from the measured major principal stress σ_1 after necking, Bridgman's analysis [19] was employed

$$\sigma_{\text{eq}} = \frac{\sigma_1}{\left(1 + \frac{2R}{a}\right) \cdot \ln\left(1 + \frac{a}{2R}\right)} \tag{4}$$

The relation between the radius of the specimen's cross-section at the root of the neck, a, and the radius of the neck profile, R, was estimated by the empirical relation proposed by Le Roy et al. [20]

$$\frac{a}{R} = 1.1 \cdot \left(\varepsilon_{\text{eq}} - \varepsilon_U\right) \tag{5}$$

valid for $\varepsilon_{\text{eq}} > \varepsilon_U$ where ε_U is the equivalent plastic strain at the onset of necking. The Bridgman corrected equivalent stress is shown as a dashed line in Fig. 2, and was used to calibrate the model in Eq. (2) by a least squares fitting of the material constants, which are listed in Tab. 1. Other approaches like inverse modelling or optical measurement techniques are possible [21]. Fracture was not observed in the component tests, and is hence not accounted for in the model. Details regarding fracture in this material can be found elsewhere [11, 22].

TABLE 1. MATERIAL CONSTANTS USED FOR CONSTITUTIVE RELATION IN NUMERICAL SIMULATIONS [23].

Elasticity and density			**Yield stress, strain hardening**		
E [MPa]	ν [-]	ρ [kg/m^3]	A [MPa]	B [MPa]	n [-]
208 000	0.33	7 800	465.5	410.8	0.4793

COMPONENT TESTS

The component tests are designed to emulate the denting and hooking of a pipeline, where the global force-displacement curves and deformation profiles of the pipes are main response parameters of interest. Data from the tests are later compared with numerical simulations.

Setup

A rig capable of applying an axial load while at the same time bending a specimen transversely has been used to test the X65 steel pipes. Two horizontal hydraulic actuators apply the axial load as indicated by the arrows in Fig. 3, while a third vertical

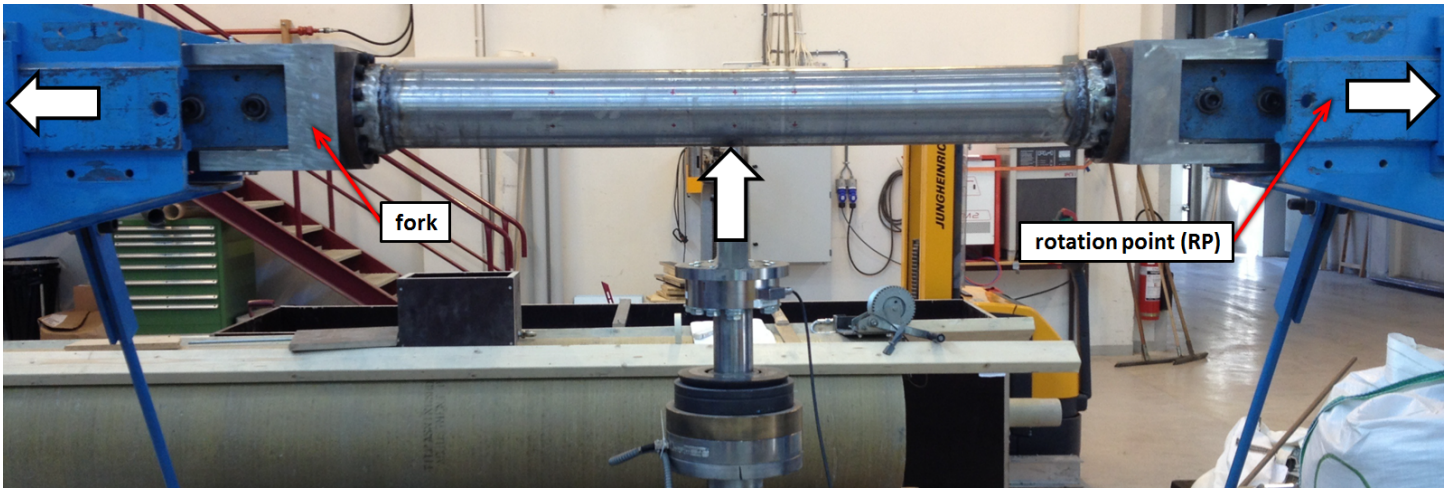

FIGURE 3. EXAMPLE OF TEST COMPONENT MOUNTED IN STRETCH-BENDING RIG, WITH THE WIDE WHITE ARROWS SIGNIFYING THE DIRECTION OF THE APPLIED LOADS. THE AXIAL LOAD IS APPLIED ON BOTH SIDES AT THE ROTATION POINTS, WHICH ARE HIDDEN BEHIND STRUCTURAL PARTS OF THE RIG.

TABLE 2. TEST MATRIX OF PIPES SUBJECTED TO COMBINED QUASI-STATIC STRETCHING AND BENDING. SEE FIG. 4 FOR LEGEND AND ILLUSTRATION.

Pipe		**A1**	**A2**	**A3**	**P1**	**P2**	**P3**
Nose radius	[mm]	10	10	10	10	10	10
Nom. transverse def.	[mm]	200	200	200	200	200	200
Avg. thickness	[mm]	4.19	4.19	4.06	4.08	3.95	4.13
Nom. overpressure	[bar]	0	0	0	100	100	100
Nom. axial load	[kN]	0	53 const.	0-53 linear	0	53 const.	0-53 linear
				Test results			
Transverse def.	[mm]	197	201	202	200	200	200
w_i	[mm]	120	120	122	117	159*	113
Horizontal def.	[mm]	15	13	13	16	14	13
$L_{\text{N-N}}$	[mm]	1200	1197	1198	1200	1168*	1200
Force at peak	[kN]	40.7	45.9	40.6	47.5	52.0	51.0
Max. vert. force	[kN]	40.7	47.0	45.7	47.5	64.1	65.4
Angle at RP	[deg]	8.7	8.5	8.7	9.6	11.6*	9.2
Angle at fork	[deg]	8.8	8.4	8.7	9.3	11.4*	8.9
Avg. axial force	[kN]	0.8†	53.0	-	0.7†	53.2	-
Avg. overpressure	[bar]	0	0	0	103	103	101
$d_{\text{N-S}}$	[mm]	84	89	87	98	90*	97
$d_{\text{E-W}}$	[mm]	164	165	164	152	164*	152
				Simulation results			
Horizontal def.	[mm]	16.4	15.8	16.0	16.1	15.4	15.5
$L_{\text{N-N}}$	[mm]	1209	1210	1210	1210	1211	1211
Force at peak	[kN]	42.3	46.4	41.6	50.2	54.0	53.2
$d_{\text{N-S}}$	[mm]	76	77	77	93	93	93
$d_{\text{E-W}}$	[mm]	167	167	167	156	156	156

*Post-test geometric measurements are inaccurate due to an erroneously applied compressive force.
†Force required to pull the horizontal pistons out.

actuator bends the pipe transversely using deformation control. Both the load and the displacement in the actuators were logged continuously during the entire test sequence. The indenter shape on the vertical actuator has the sharpest nose radius (10 mm) given the DNV GL guidelines [24]. The applied transverse displacement is 200 mm (at a deformation rate of 25 mm/min) is the same for all tests, while the axial load varies between three cases. The first and simplest is no axial load at all, while the second case is a constant axial load of about 53 kN. Finally, the third axial load is increasing linearly from 0 kN to 53 kN simultaneously as the transverse deformation increases from 0 mm to 200 mm. The applied axial load is well below the calculated elastic limit, and was chosen based on simplified simulations using beam elements. Three cases will be tested without pressure (pipes A1-A3), and three will be tested with an internal pressure of approximately 100 bar (pipes P1-P3). The component test matrix is shown in Tab. 2, along with some test parameters and both experimental and numerical results.

The pipes were initially about 10 mm thick, but were lathed down to about 4 mm in the test section (length 1000 mm) to obtain a diameter to thickness ratio of about 30 which is more common and the same as in the Kvitebjørn accident [13]. This lathing may cause a slightly uneven thickness, so the thickness of each pipe is therefore measured across several points, from which an average thickness is estimated. The inner diameter of the pipes is about 123 mm, and the initial span between the rotation points on the rig (see Fig. 3) is approximately 2.1 m, whereas the specimens themselves were only 1250 mm long. The additional length to the span comes from the somewhat convoluted connection required to fit the circular geometry of the pipes to the rig while allowing application of an internal pressure.

As mentioned, six tests were conducted in total, using three different axial loads with and without internal pressure. The following test procedure was applied for each pipe:

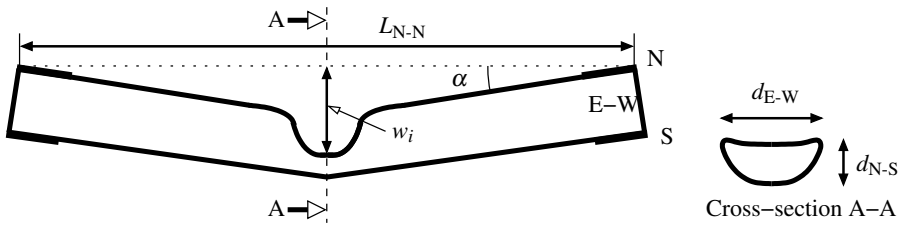

FIGURE 4. TYPICAL OUTLINE OF DEFORMATION SHAPE (NOT TO SCALE) OF PIPES AFTER TESTING, ALONG WITH EXPLANATION OF MEASUREMENTS GIVEN IN TABLE 2.

1. Application of internal pressure (if relevant).
2. Application of constant horizontal load (if relevant).
3. (a) Application of transverse displacement of 200 mm.
   (b) Simultaneous application of linearly increasing horizontal load (if relevant).
4. Locking of horizontal actuators.
5. Removal of vertical indenter.
6. Unloading of horizontal actuators.

Unloading of the pipes was done slowly to prevent dynamic springback, as this is intended to be a quasi-static test. During testing, the horizontal and vertical forces and displacements were logged, as were the angles of the pipe at the rotation points and the pressure inside the pipe. Digital image correlation (DIC) was attempted with varying degrees of success, and discussion of those results are omitted for brevity.

Water was used to pressurise the pipes, and pressure was applied using a pump continuously working throughout the test procedure. A valve automatically opening at approximately 100 bar kept the pressure in the system constant even as the volume of the pipes decreased during deformation. In a real case, where the pipelines may span many kilometers, such a small relative change in volume due to a dent would not alter the pressure notably.

Results

A typical outline of a deformed pipe is sketched in Fig. 4. Transverse force-displacement curves are shown in Fig. 5, with 5(a) containing the data from the experiments with no internal overpressure, and 5(b) showing the resulting force-displacement curves when an additional internal overpressure of about 100 bar was applied to the pipe.

The force-displacement curves show a stiffer response when internal pressure is included. Now a pronounced difference in cross-sectional deformation is noted as well, with the pressurised pipes having a more localised final deformation in accordance with other works [25–27]. Pictures of this observation are shown in Fig. 6, where the top row shows the dent in the pipe after being deformed without pressure, and the bottom row with an

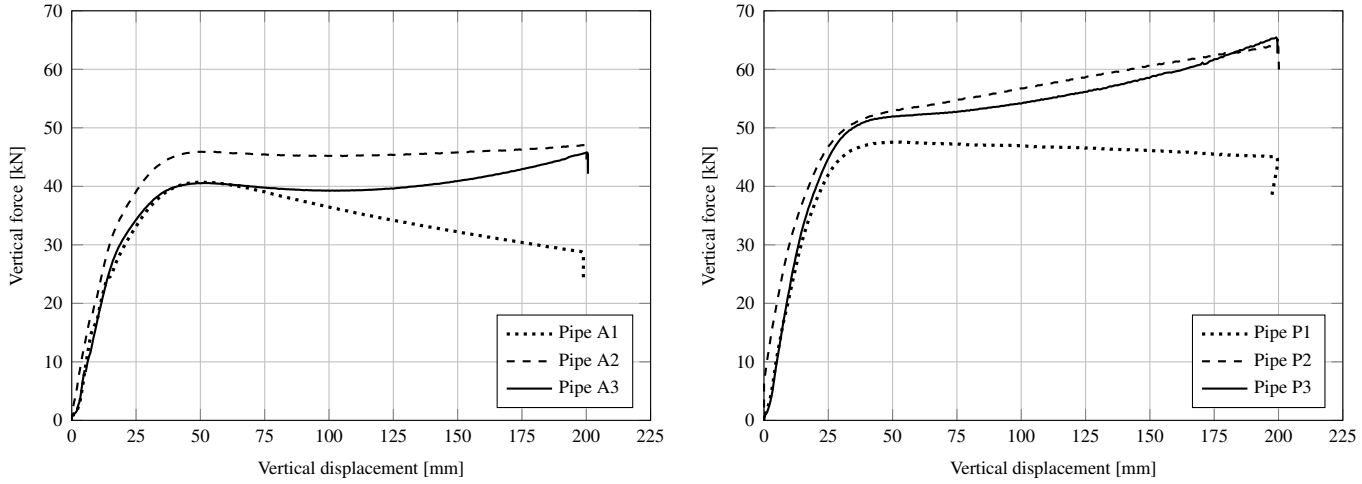

(a) No pressure

(b) Pressure = 100 bar

FIGURE 5. TRANSVERSE FORCE-DISPLACEMENT CURVES FROM (a) THE UNPRESSURISED PIPES A1-A3, AND (b) THE PRESSURISED PIPES P1-P3.

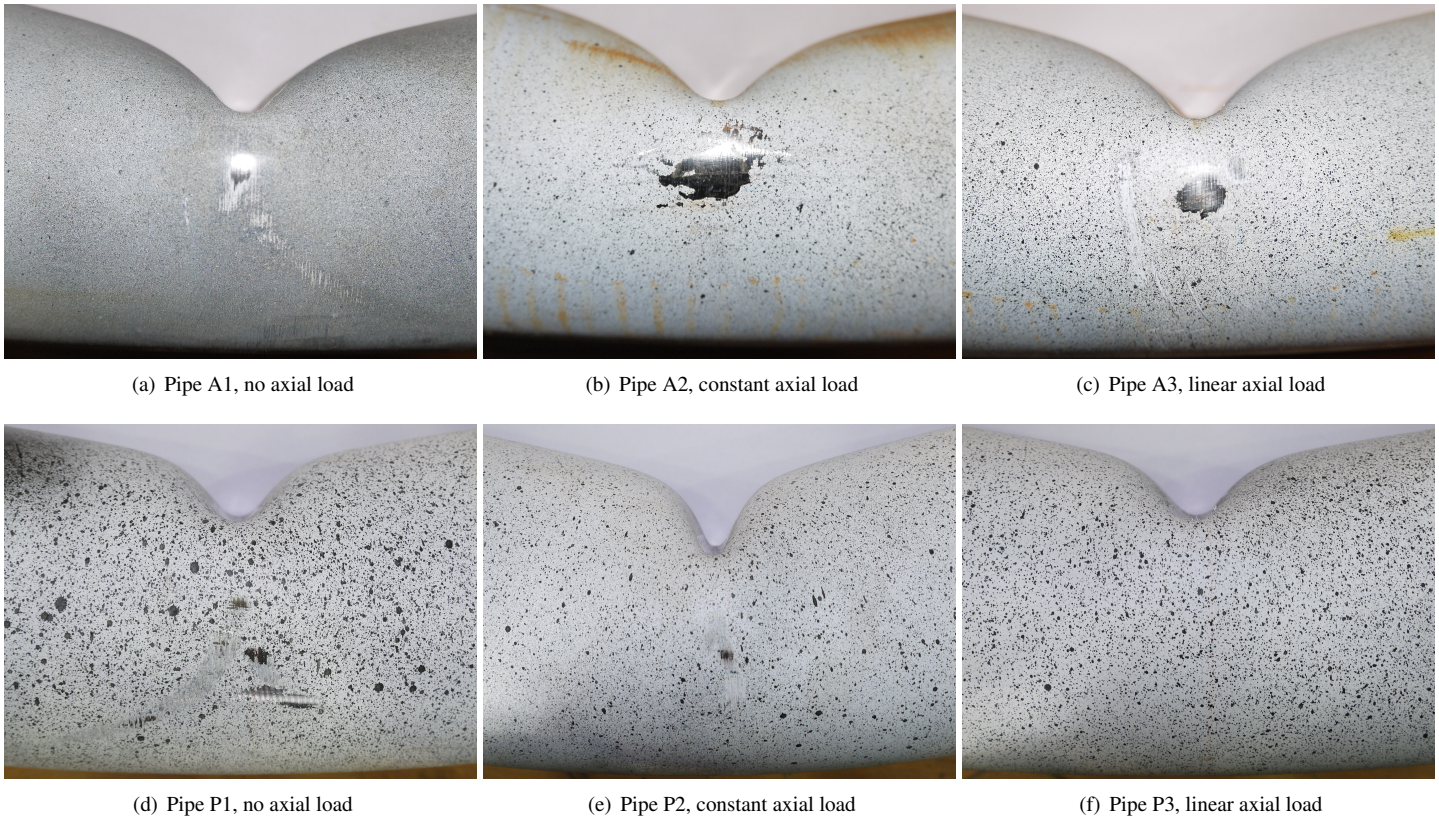

(a) Pipe A1, no axial load (b) Pipe A2, constant axial load (c) Pipe A3, linear axial load

(d) Pipe P1, no axial load (e) Pipe P2, constant axial load (f) Pipe P3, linear axial load

FIGURE 6. LOCAL DEFORMATION IN DENT WITHOUT PRESSURE (TOP ROW) AND WITH APPROXIMATELY 100 BAR PRESSURE (BOTTOM ROW). THE LEFT COLUMN HAS NO AXIAL LOAD, THE MIDDLE COLUMN HAS A CONSTANT AXIAL LOAD, WHILE THE RIGHT COLUMN HAS A LINEARLY INCREASING AXIAL LOAD. THE PAINT DOTS SEEN WERE APPLIED AS CONTRAST FOR DIC.

internal overpressure. As observed, the "diameter" from top to bottom ($d_{\text{N-S}}$ from Fig. 4) is greater in magnitude when pressure is included (see Tab. 2). This may of course alter not only the magnitude of strains but also the strain path and stress triaxiality, which can be quite important when discussing fracture [22]. Reducing the dent size is beneficial as the load bearing capacity drops quickly when a dent exceeds 5% of the outer diameter [28]. Note that pipe P2, part (e) in Fig. 6, was compressed by an unintentional axial load after the test due a bug in the rig's software, resulting in a final deformation not representative for the described load sequence (the dent became even sharper). For this reason, a direct comparison of the measured cross-sectional deformation from pipe P2 with values from the other pipes is not applicable.

From Fig. 5 it is also deemed that a constant axial load increases the pipe's resistance to bending, meaning that the force to produce an equivalent deformation without the axial load is lower. The linearly increasing axial load has the same effect, and the effect is greater for larger values of the axial load in line with expectations. Further, the local cross-sectional deformation appears much less affected by the axial load. In terms of final local deformation, it was hard to distinguish between the three different tensile axial load configurations, whereas a compressive axial load (not investigated herein) can reduce the lateral collapse load significantly [29]. In general, the test are repeatable and consistent and should represent the main physics of the problem. As previously mentioned, fracture is not studied in detail here. It is, however, noted that no fracture was observed in these pipes after the prescribed load sequence.

NUMERICAL SIMULATIONS

Setup

The simulations carried out herein are numerical versions of the component tests. First, the experiments without pressure are recreated (A1-A3), and then pressure is included in an otherwise identical simulation (P1-P3). All simulations have been carried out using the commercially available finite element software ABAQUS [14], and the simulations are run with explicit time integration as contact is an important part of the analysis.

Fig. 7 shows a sketch of the numerical setup. Four-node, re-

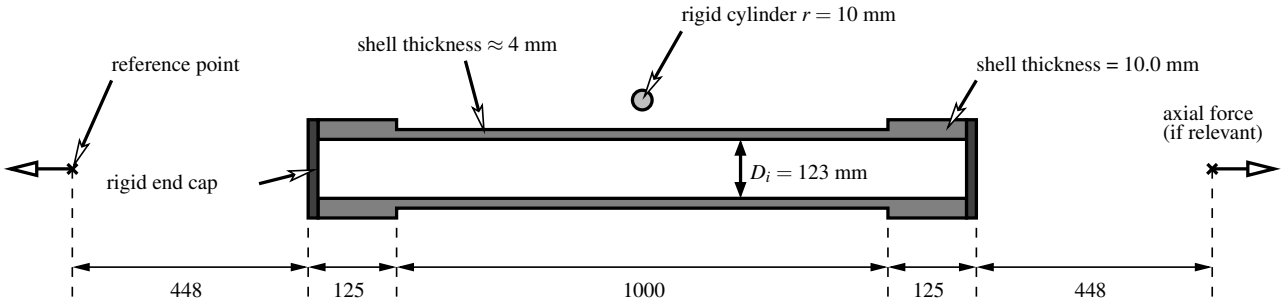

FIGURE 7. SKETCH OF THE SETUP FOR THE FINITE ELEMENT SIMULATIONS.

duced integration shell elements (called `S4R` in ABAQUS) with five integration points in the thickness direction are used to model the pipe. The midsection of the pipe has a uniform shell thickness of about 4 mm (varies for each pipe) for the entire length of 1000 mm, while the end sections are set to be 10.0 mm thick. To each end section a rigid cap is attached to represent the "forks" attaching the pipe to the hydraulic pistons shown in Fig. 3. The reference points for these rigid caps are made to coincide spatially with the rotation points in the rig, thereby allowing the ends of the pipe to rotate as in the experiments. These reference points (see Fig. 7) are restricted to move only in the axial direction of pipe, representing the movement of the pistons. When relevant, the axial loads are applied to these points as in the experiments.

Further, rigid elements were used to represent the indenter. A cylinder with radius 10 mm was chosen, a representation which has been shown to work well [23]. It is placed directly above the pipe, and given a constant velocity of 0.42 mm/s throughout the analyses like in the experiments. The sequential procedure is basically the same as described above for the physical experiments. Pressure is always applied first in a separate step with a duration of 10 s, along with the constant axial load (if relevant). Then the indenter is set in motion normal to the pipe's axis, and the axial load increases linearly along with the indenter displacement (if relevant). In the simulations of pressurised pipes the pressure is always uniform as measured in the experiments (see Tab. 2), and the pressure is applied to the surface of the end sections and the end caps to keep the pressure from creating an uneven force balance when the rotation becomes larger.

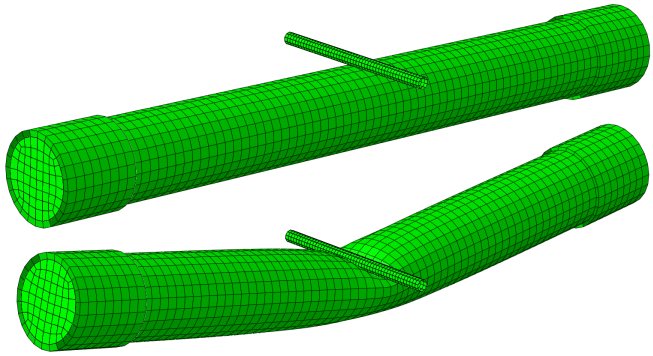

FIGURE 8. UNDEFORMED MESH (TOP) USED IN FINITE ELEMENT SIMULATIONS, AND A DEFORMED MESH (BOTTOM).

As mentioned, the experiments are quasi-static and take almost 500 s to complete. This naturally results in time comsuming simulations (see Tab. 3), necessitating some degree of mass scaling. A mesh with 16 elements across the circumference and 42 along the 1000 mm midsection is used for the mass scaling simulations, and five different mass scaling factors were used (1, 10^2, 10^4, 10^6, and 10^8). The results of this endeavor are listed in Tab. 3, and a fair compromise between speed and accuracy is attained at a mass scaling factor of 10^4 as the discrepancy from the simulation with no mass scaling was less than 1%. Using double precision was crucial to avoid accumulating errors as the number of iterations became very high in the most extreme cases. For the final simulations, a mesh size of 24 elements along the cir-

TABLE 3. RESULTS FROM MASS SCALE STUDY ON PIPE MESH WITH 16×42 ELEMENTS IN THE MIDSECTION.

Factor	**Iterations**	F_{peak} [kN]	$\bar{F}$ [kN]	$\Delta\bar{F}$ [kN]	$\Delta\bar{F}/F_{\text{peak}}$	$E_{\text{kin}}/E_{\text{tot}}$	**Time** [hh:mm:ss]
1	134 508 429	45.8	37.7	0.0	0.0%	0.0%	36:58:03
10^2	13 450 905	45.9	37.7	0.1	0.3%	0.0%	03:55:51
10^4	1 396 965	46.8	37.8	0.3	0.8%	0.0%	00:20:05
10^6	134 206	48.6	38.0	1.0	2.6%	0.8%	00:02:17
10^8	13 378	80.6	38.6	5.8	15.0%	70.1%	00:00:12

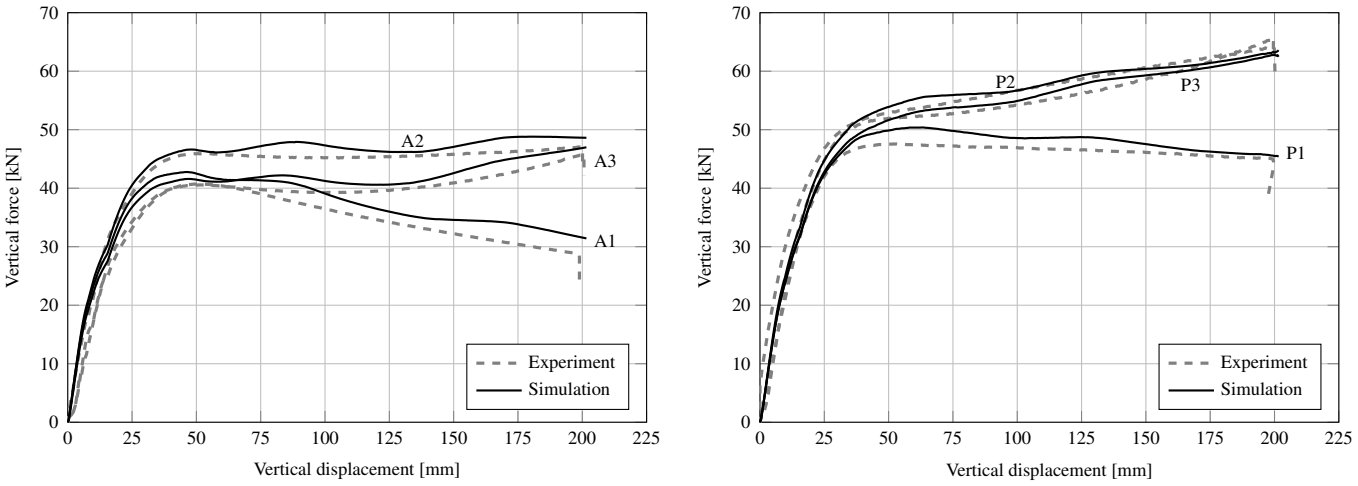

(a) No pressure (b) 100 bar pressure

FIGURE 9. TRANSVERSE FORCE-DISPLACEMENT CURVES FROM SIMULATIONS OF (a) THE UNPRESSURISED PIPES A1-A3, AND (b) THE PRESSURISED PIPES P1-P3.

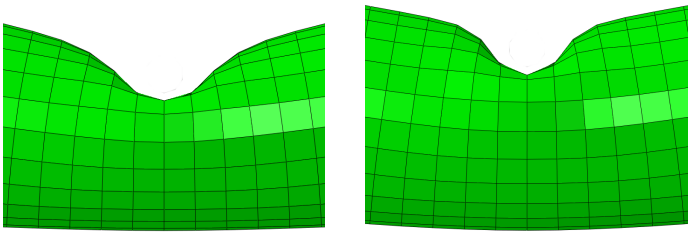

(a) No pressure (b) 100 bar pressure

FIGURE 10. NO PRESSURE VS. PRESSURE.

cumference and 62 along the 4 mm thick middle section of the pipe, resulting in an element side length of approximately 16 mm which has been shown to yield good results [23]. The mesh with the shell thickness rendered is shown in Fig. 8.

Results

The main goal of the simulations was to capture the global behaviour of the pipes in terms of transverse force-displacement curves, and this has been done with good accuracy as shown in Fig. 9. The initial stiffness, i.e., the initial tangent of each curve, was matched quite well by the simulation results. Adding an axial load to the rotation points increases the force level in accordance with the experimental results. An important parameter for the pipe's bending resistance is the thickness, which in the experiments varies not only between each pipe, but also within each pipe. The effect of uneven thickness is not included in the simulations, and could result in some discrepancy between the numerical and experimental results. The increase in force due to the internal overpressure was adequately captured, in line with the numerical work by Dou and Liu [30]. The effect of pressure on the final deformation of the cross-section is also well represented, as shown in Fig. 10. Values of $d_{\text{N-S}}$ and $d_{\text{E-W}}$ are also fairly well predicted, where the error when measuring the physical pipes can make an influence due to the shape of the deformed cross-section (see Tab. 2 and Fig. 4). As in the experiments, it is difficult to see any significant difference in the final deformation due to the different axial loads.

In Fig. 9, a slightly wavy shape of the force-displacement curves is noted. This is partly due to some dynamic effects being present due to mass scaling [31], and partly due to the sequential initiation of contact between the pipe and indenter. As each circumferential row of elements come into contact with the indenter, and slight increase in the tangent of the force-displacement curve is noted. By employing a finer mesh, this effect can be rectified. Generally, the simulations are able to represent the experiments well with reasonable time consumption (about 1 hour).

DISCUSSION AND CONCLUDING REMARKS

The X65 material used in the pipes is both isotropic and homogeneous [11], and the chosen material model appears to provide sufficient accuracy for the global simulations. Component tests show that including an internal pressure increases the force required to reach a certain deformation. Also, the cross-sectional shape is less deformed after the test procedure, with a more localised dent as noted in previous work [8].

Applying a constant axial force further increases the force when deforming the pipe transversely. Application of an ax-

ial load which increases linearly with the transverse deformation shows that the effect of increased resistance is greater for greater values of the axial load, which is in line with expectations. It was difficult to detect any difference in final deformation due to the different axial loads.

The finite element simulations conducted were able to capture the global behaviour quite well, both in terms of force-displacement curves and initial system stiffness. The effects of the axial load and of the pressure were captured adequately, and the final deformation of the cross-section was predicted reasonably well.

ACKNOWLEDGMENT

The present work has been carried out with financial support from the Research Council of Norway SIMLab – Centre for Research based Innovation (CRI) at the Norwegian University of Science and Technology. Thankful acknowledgement is made to Statoil ASA for supplying the pipes.

REFERENCES

[1] Jones, N., and Birch, R., 2008. "Impact behaviour of pressurised pipelines". *Structures Under Shock and Impact X*, pp. 219–228.

[2] Longva, V., Sævik, S., Levold, E., and Ilstad, H., 2013. "Dynamic simulation of subsea pipeline and trawl board pull-over interaction". *Marine Structures,* ***34***, pp. 156–184.

[3] Liu, B., and Soares, C., 2015. "Plastic response and failure of rectangular cross-section tubes subjected to transverse quasi-static and low-velocity impact". *International Journal of Mechanical Sciences,* ***90***, pp. 213–227.

[4] Wang, Z., Liu, K., Ji, C., Chen, D., Wang, G., and Soares, C., 2016. "Experimental and numerical investigations on the T joint of jack-up platform laterally punched by a knife edge indenter". *Ocean Engineering,* ***127***, pp. 212–225.

[5] Jones, N., Birch, S., Birch, R., Zhu, L., and Brown, M., 1992. "An experimental study on the lateral impact of fully clamped mild steel pipes". *Proceedings of the Institution of Mechanical Engineers, Part E: Journal of Process Mechanical Engineering*, pp. 111–127.

[6] Soares, C., and Søreide, T., 1983. "Plastic Analysis of Laterally Loaded Circular Tubes". *Journal of Structural Engineering,* ***109***, pp. 451–467.

[7] Travanca, J., and Hao, H., 2014. "Numerical analysis of steel tubular member response to ship bow impacts". *International Journal of Impact Engineering,* ***64***, pp. 101–121.

[8] Jones, N., and Birch, R., 1996. "Influence of internal pressure on the impact behaviour of steel pipelines". *International Journal of Pressure Vessel Technology,* ***118***, pp. 464–471.

[9] Shen, W., and Shu, D., 2002. "A theoretical analysis on the failure of unpressurised and pressurised pipelines". *Proceedings of the Institution of Mechanical Engineers 216 (E)*, pp. 151–165.

[10] Manes, A., Porcaro, R., Ilstad, H., Levold, E., Langseth, M., and Børvik, T., 2012. "The behaviour of an offshore steel pipeline material subjected to stretching and bending". *Ships and Offshore Structures,* ***7***, pp. 371–387.

[11] Kristoffersen, M., Børvik, T., Westermann, I., Langseth, M., and Hopperstad, O., 2013. "Impact against X65 steel pipes — An experimental investigation". *International Journal of Solids and Structures,* ***50***, pp. 3430–3445.

[12] Kristoffersen, M., Børvik, T., Langseth, M., and Hopperstad, O., 2016. "Dynamic versus quasi-static loading of X65 steel pipes". *European Physical Journal – Special Topics,* ***225***, pp. 325–334. DOI: 10.1140/epjst/e2016-02629-4.

[13] Kristoffersen, M., 2014. "Impact against X65 offshore pipelines". PhD thesis, Norwegian University of Science and Technology.

[14] SIMULIA, 2016. *Abaqus user's manual version 6.14*.

[15] Oh, C.-K., Kim, Y.-J., Baek, J.-H., and Kim, W.-S., 2007. "Development of stress-modified fracture strain for ductile failure of API X65 steel". *International Journal of Fracture,* ***143***, pp. 119–133.

[16] Ghiotti, A., Fanini, S., Bruschi, S., and Bariani, P., 2009. "Modelling of the Mannesmann effect". *CIRP Annals - Manufacturing Technology,* ***58***, pp. 255–258.

[17] Fourmeau, M., Børvik, T., Benallal, A., and Hopperstad, O., 2013. "Anisotropic failure modes of high-strength aluminium alloy under various stress states". *International Journal of Plasticity,* ***48***, pp. 34–53.

[18] Kristoffersen, M., Børvik, T., Langseth, M., Ilstad, H., Levold, E., and Hopperstad, O., 2013. "Damage and failure in an X65 steel pipeline caused by trawl gear impact". *Proceedings of the ASME 2013 32nd International Conference on Ocean, Offshore and Arctic Engineering*.

[19] Hill, R., 1950. *The Mathematical Theory of Plasticity*. Oxford University Press.

[20] Le Roy, G., Embury, J., and Ashby, M., 1981. "A model of ductile fracture based on the nucleation and growth of voids". *Acta Metallurgica,* ***29***, pp. 1509–1522.

[21] Ehlers, S., and Varsta, P., 2009. "Strain and stress relation for non-linear finite element simulations". *Thin-Walled Structures,* ***47***, pp. 1203–1217.

[22] Kristoffersen, M., Børvik, T., and Hopperstad, O., 2016. "Using unit cell simulations to investigate fracture due to compression-tension loading". *Engineering Fracture Mechanics,* ***162***, pp. 269–289.

[23] Kristoffersen, M., Casadei, F., Børvik, T., Langseth, M., and Hopperstad, O., 2014. "Impact against empty and water-filled X65 steel pipes – Experiments and simula-

tions". *International Journal of Impact Engineering,* ***71***, pp. 73–88.
[24] DNV GL AS, 2014. *Offshore standard DNV-RP-F111: Interference between trawl gear and pipelines*. Det Norske Veritas Germanischer Lloyd AS.
[25] Jones, N., and Birch, R., 2010. "Low-velocity impact of pressurised pipelines". *International Journal of Impact Engineering,* ***37***, pp. 207–219.
[26] Shah, Q., 2011. "Experimental and numerical study on the orthogonal and oblique impact on water filled pipes". *International Journal of Impact Engineering,* ***38***, pp. 330–338.
[27] Iflefel, I., Moffat, D., and Mistry, J., 2005. "The interaction of pressure and bending on a dented pipe". *International Journal of Pressure Vessels and Piping,* ***82***, pp. 761–769.
[28] Baek, J.-H., Kim, Y.-P., Kim, W.-S., Koo, J.-M., and Seok, C.-S., 2012. "Load bearing capacity of API X65 pipe with dent defect under internal pressure and in-plane bending". *Materials Science and Engineering A,* ***540***, pp. 70–82.
[29] Zeinoddini, M., Harding, J., and Parke, G., 1998. "Effect of impact damage on the capacity of tubular steel members of offshore structures". *Marine Structures,* ***11***, pp. 141–157.
[30] Dou, Y., and Liu, Y., 2015. "Computational investigation of lateral impact behavior of pressurized pipelines and influence of internal pressure". *Thin-Walled Structures,* ***95***, pp. 40–47.
[31] Kristoffersen, M., Børvik, T., Langseth, M., and Hopperstad, O., 2015. "X65 steel pipes subjected to combined stretching and bending". *MARINE 2015 - Computational Methods in Marine Engineering VI*, pp. 1004–1014.